PEM ELECTROLYSERS FOR OPERATION WITH
OFFGRID RENEWABLE INSTALLATIONS

Development of subsystems for offgrid integration

Deliverable 4.1

D4.1 Development of subsystems for offgrid integration

Grant agreement	Fuel Cells and Hydrogen 2 Joint Undertaking
Project no.	700359
Project full title	PEM ElectroLYsers FOR operation for OFFgrid renewable facilities
Project acronym	ELY4OFF
Deliverable no.	4.1
Title of deliverable	Development of subsystems for offgrid integration
Contractual date of delivery	M14
Actual date of delivery	M
Author(s)	Sergio Ayuso (INYCOM), Guillermo Matute (INYCOM)
Participant(s)	Nick van Dijk (ITM), Helio Bustamante (ITM), Logan López (EPIC), Rubén Gálvez (EPIC), Eduardo Morales (INYCOM), Iván Lalaguna (INYCOM)
Work Package contributing to the deliverable (WPx)	WP4
Dissemination level (PU/CO/CI)	PU
Type (R/DEM/DC/OTHER)	R
Total number of pages	44

Abstract summary

This report provides a description of the components and subsystems which allow the integration of the ITM Power PEM water electrolyser (PEMWE) with the remaining elements in the facilities of the Foundation for the Development of New Hydrogen Technologies in Aragon (FHA), as requested in the ELY4OFF Grant Agreement No.700359. These elements are: (1) the power electronics (PE) developed by EPIC to directly couple the PEMWE to the photovoltaics (PV) installation at FHA (DC/DC converter), as well as (2) the overarching control and communication system (C&CS) developed by INYCOM to optimize the overall installation.

Some changes may be added over the provisions of the document considering the fact that additions could come from other tasks' developments (especially in WP4).

Table of contents

1. <u>Introduction</u>

The European Union has set ambitious targets related to energy efficiency, renewable energy and greenhouse gases emissions to reach long term climate change goals. By 2030 the EU aims to reduce GHG emissions by 40%, to increase the share of RE in the member states energy mix to 27%, and to reach a 27% energy efficiency target [1]. To accommodate this share of RES without overloading transmission and distribution grids, a techno-economically viable solution is the conversion of surplus renewable energy into hydrogen which may be used in a wide range of applications [2], [3]: (1) chemical industry, to generate other products, (2) fuel cell electric vehicles refueling, (3) injection into the natural gas grid, using gas networks as storage system for electric grids, and (4) re-electrification to inject electricity in weak grids where faults are common or in isolated microgrids where access to the main grid is not possible and a combination of RES and fossil fuel based generation is present.

The fourth scenario, with offgrid generation of hydrogen from RES is especially attractive because: (a) it allows replacement of diesel engines in isolated regions to back-up the existing RES and there are currently 600 GW available for substitutions worldwide, (b) global efficiency is not a key issue as in the case of grid connected systems, as hydrogen is produced avoiding curtailed energy that would be otherwise wasted, (c) hydrogen uses are varied and not only re-injection can be studied, but also feeding FCEVs or stationary fuel cells to cover also heat demand, (d) hydrogen is competitive with other energy storage equipment such as electrochemical batteries which show problems related to self-discharging and maintenance in the case of seasonal storage, offering long-term security of supply.

However, state of the art electrolysers still show margin for incremental improvements to be technically adapted to fully offgrid operation while being cost-competitive. PEM water electrolysis (PEMWE) is a very promising option due to its dynamic response behavior which is of key importance for direct coupling to RES. ELY4OFF relies on PEM technology to show that PEMWE are able to be directly coupled to photovoltaics (PV) to cover different demands of hydrogen by end user (mobility and stationary fuel cells to keep the system operative). The behavior of PEMWE directly connected to PV through DC/DC has been sufficiently modeled, simulated and tested in low power benches in the laboratory in the literature [4], [5], [6], [7], but ELY4OFF progress beyond showing a fully offgrid connection in real environment with a 50 kW system.

The direct coupling of the PEMWE to generation (PV), as well as its connection to the different hydrogen loads (storage, compression and hybrid storage system of FHA), requires specific subsystems for offgrid integration which are, in the case of ELY4OFF: (1) a highly efficient, reliable, fast-response and dynamic power electronics DC/DC converter (delivered by EPIC) and (2) a remotely monitored overarching control and communication system (C&CS) able to learn from the gathered signals and optimize global installation operation while keeping the equipment under safety thresholds and guaranteeing sufficient lifetime (delivered by INYCOM).

Thus, this deliverable aims to present the advances done in the subsystems for offgrid integration (PE and overarching C&CS) and shows the progress of tasks 4.1 and 4.2. Mainly, the deliverable gathers:

- The **definitive topology for the DC/DC converter** (section 2), selected considering techno-economic criteria such as devices stress, power, efficiency, control, EMC/EMI behavior and cost
- The **signals received/sent and communication protocols of the overarching C&CS** (section 3) to the equipment, the required **hardware** (section 4) as well as the **logic of operation** (section 5) of the global installation.

2. Power electronics architectures for PEMWE-PV direct connection

Following the requirements extracted from the WP2 (Requirements and LCC assessment) the first task is to analyze the best architecture for the Power Conversion subsystem. Two different approaches (with direct DC/DC vs. intermediate AC link) are going to be considered. The definition of adequate figures of merit (WP2) will lead to a correct selection of the conversion architecture (at "black box" converter level).

2.1 Figures of merit

To identify the best topology for the ELY4OFF project, several figures of merit must be identified. Many of them could be part of the document "D2.3 System capability requirements".

The identified figures of merit are:

- MPPT efficiency
- Power stages chain efficiency
- Volume
- Weight
- Cost
- Control complexity
- Redundancy

Depending on the way the solar panels are interconnected, the generated power could be different. First, due to manufacturing tolerances the installed panels show different current-voltage curves. Additionally, even if the distances between panels are small, they will not be isolated exactly with the same amount of radiation and the temperature of each particular panel can also differ. Thus, though the application of the MPPT algorithm to a solar panel gets the maximum available power at this particular panel, this is not the case when dealing with several panels connected in series or in parallel. As the panels share the same polarization point, they are not operating at their particular (and different) MPP. Because of that, the overall generated power is below the theoretical maximum power available if each panel is polarized at its particular MPP. An example is given in the following figure:
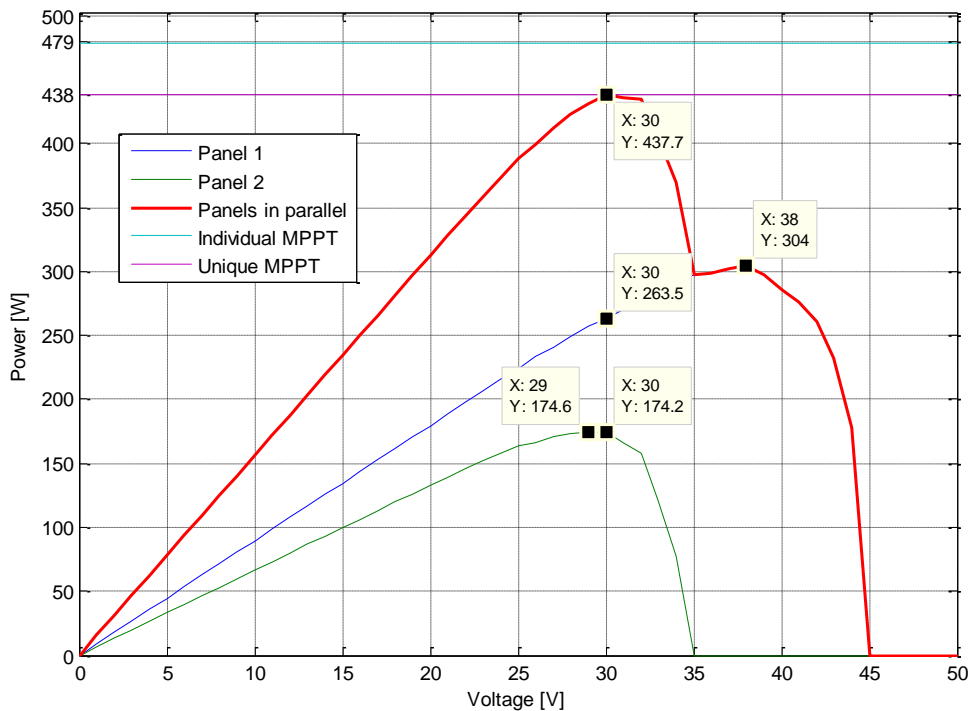
Fig. 1 Comparison between individual MPPTs vs MPPT of two paralleled panels

In this example, an 8.5% of energy is lost if panels are connected together without a power stage. Thus it can be concluded that it could be of interest to organize several independent strings of panels with several MPPT algorithms.

The main objective of this system is to obtain as much hydrogen as possible. Because of that, the efficiency should be as high as possible. Also stand-by consumptions should be taken into account.

The off-grid electrolyzer may be sent to remote areas without network. In some cases, the whole system could be transported depending on the needs of the customers. In this situation, it is important to keep the volume and weight as low as possible.

The stack is instantaneously feed by the power supplied by the solar panels. The final architecture must lead to an achievable control strategy. It will be important to face any dynamic requirement, for example, cloudy situations. Some architectures could lead to complex controls in order to keep the stability of the power conversion.

Also, redundancy is a desirable characteristic that will be helpful in cases of:

- One or several solar panels fails
- One or several power converters fails
- One or several solar panels are shadowed

2.2   Power architectures

There are two different approaches. The first one keeps the existing AC to DC equipment that feeds the electrolyser in AC grid tied systems.

The second one aims to simplify the supply chain, feeding directly the DC port of the stack with a DC to DC converter.

2.2.1   DC to AC and AC to DC architecture

This architecture aims to maintain the existing AC to DC power supply of the stack. This power supply is fed from a standard network of 3ph 400 Vac. A unique DC to AC converter with MPPT (Maximum Power Point Tracking) is needed to generate this virtual 3ph 400Vac network from the solar panels.
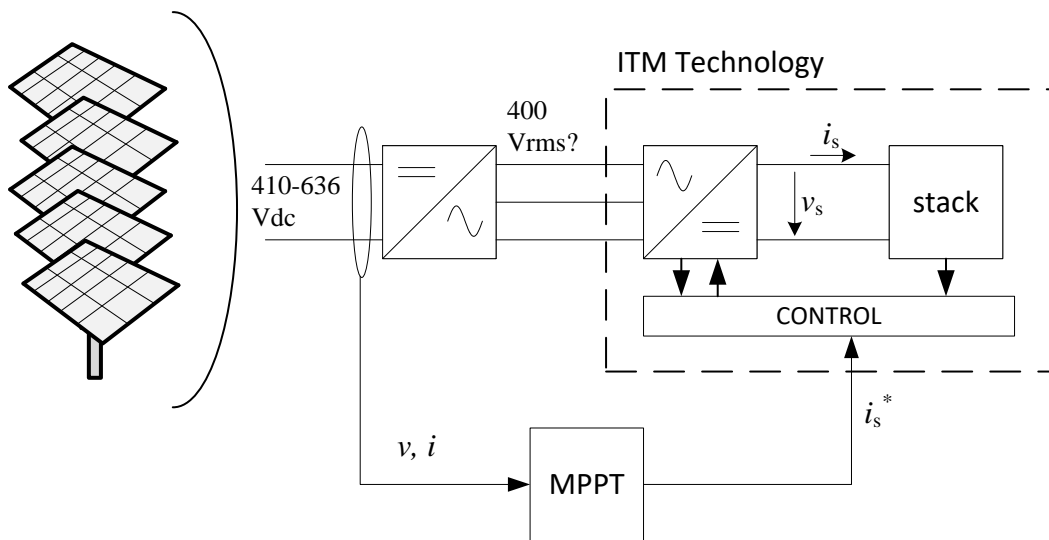

Fig. 2 DC to AC inverter in series with a AC to DC power supply

All the solar panels are connected together. This reduces the MPPT efficiency.

The key difference with a grid tied system is that there is no a network as a voltage source. This leads to perform the MPPT control through the stack power consumption. So, AC to DC power supply should have a time response in the order of microseconds or milliseconds.

Usually, a 50 Hz system incorporates LCL filters to meet current and voltage THD (Total Harmonic Distortion) requirements. This filters use to be heavy, big and relatively expensive.

There are two converters in series, so efficiency will be reduced. Besides, if one of them fails, hydrogen production will be stopped.

2.2.2   Parallelized DC to AC and AC to DC architecture

This architecture aims to maintain the existing AC to DC power supply of the stack. This power supply is fed from a standard network of 3ph 400 Vac. Several DC to AC converters with MPPT will be parallelized to generate a 3ph 400Vac network from the solar panels.
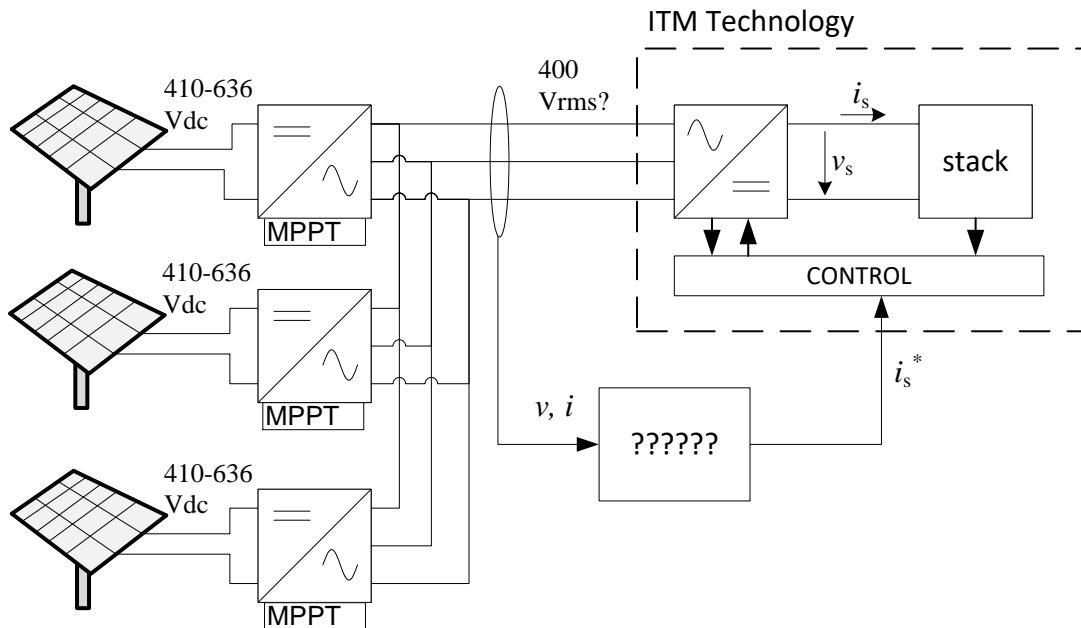
Fig. 3 Several parallelized DC to AC inverters in series with a AC to DC power supply

There are two stages in series, so efficiency will be reduced. Unlike the previous architecture, having a segregated solar panel distribution improves MPPT efficiency. As the previous architecture, the control is achieved through several systems (DC to AC and AC to DC).

The presence of the 50 Hz AC network increments the cost (also volume and weight) due to the heavy low frequency filters. Regarding redundancy, if the AC to DC fails, hydrogen production will be stopped.

2.2.3   DC to AC and AC to DC architecture with parallelized DC to DC

This architecture aims to maintain the existing AC to DC power supply of the stack. This power supply is fed from a standard network of 3ph 400 Vac. A unique DC to AC converter with MPPT is needed to generate a 3ph 400Vac network from the solar panels. This DC to AC converter is fed with several DC to DC converters. This architecture is similar to *2.2.1 DC to AC and AC to DC architecture*, but the solar panel interconnection is performed by DC to DC converters. These architecture optimizes the MPPT efficiency.
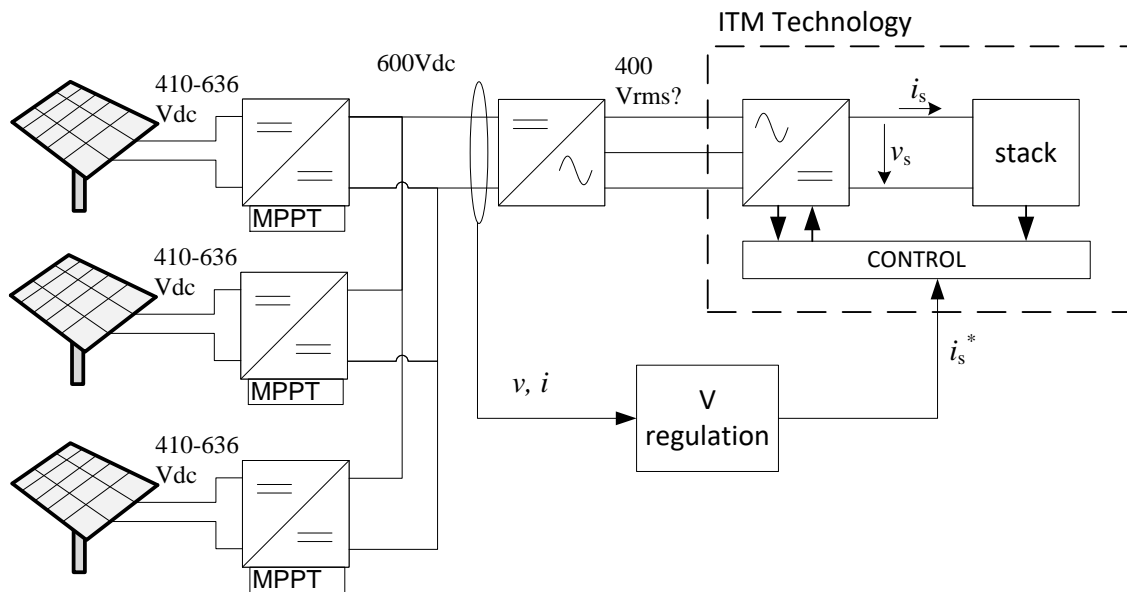
Fig. 4 DC to AC inverter with previous DC to DC stage and with a AC to DC power supply in series

However, there are three converters in series. So efficiency will be lower than previous architectures.

Besides, a complex control must set the current consumption of the AC to DC power supply that feeds the stack. This control must be fast enough to stabilize an intermediate DC link.

Regarding redundancy, if the AC to DC fails, hydrogen production will be stopped.

2.2.4 DC to DC architecture

This architecture removes the existing AC to DC power supply to optimize the power conversion chain. A direct DC to DC conversion is performed in order to improve the system efficiency.

A 50 Hz AC network is not implemented, so low frequency LCL filters are eliminated. Thereby volume, weight and probably also cost are reduced.

Fig. 5 DC to DC architecture

All the solar panels are connected together. This reduces the MPPT efficiency.

Besides, if this unique DC to DC or one of the solar panels fail, hydrogen production will be stopped.

2.2.5   Parallelized DC to DC architecture

This architecture removes the existing AC to DC power supply to optimize the power conversion chain. A direct DC to DC conversion is performed in order to improve the system efficiency.

A 50 Hz AC network is not implemented, so low frequency LCL filters are eliminated. Thereby volume, weight and probably also cost are reduced.
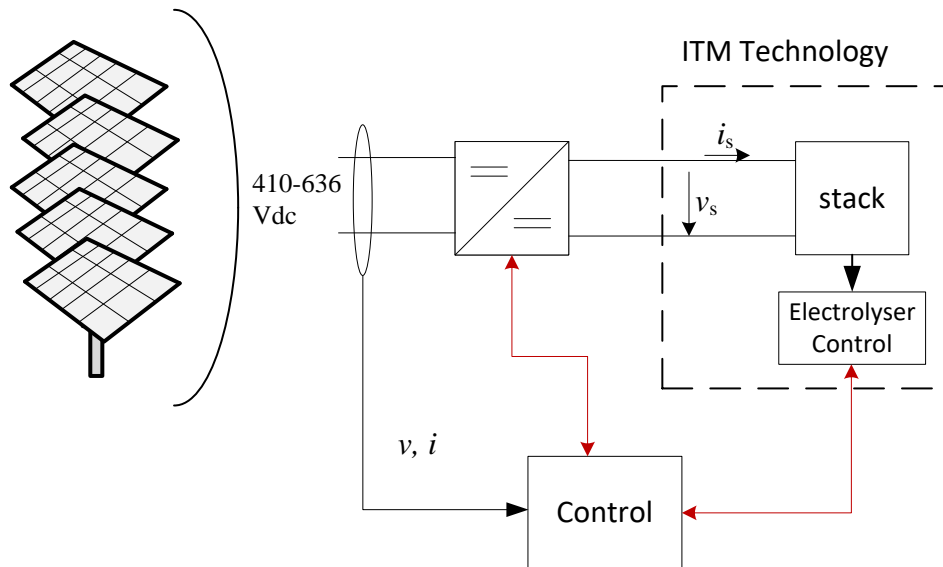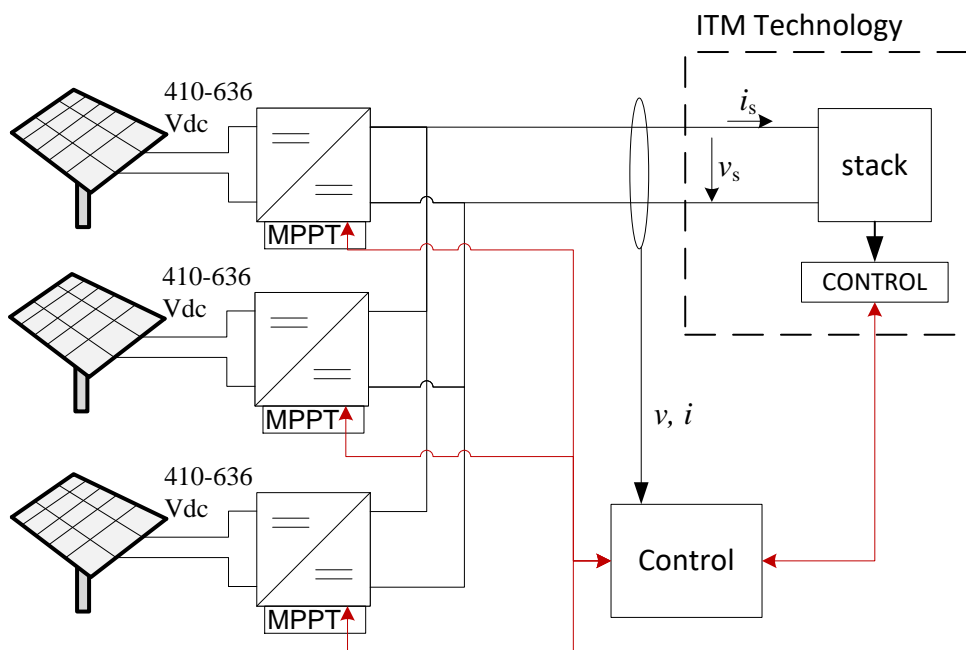

Fig. 6 Parallelized DC to DC architecture

There are several converters interfacing with the stack. Because of that, if some of them is not working as desired, the stack can still be fed through the other converters. As explained before, this redundancy lets the system be operative in some failure situations.

Each array could be connected to a different converter. This improves the efficiency of the MPPT algorithm. The number of solar cells in series can be adjusted to reduce cable costs. The higher the voltage, the lower the current. The lower the current, the lower the section of the cables.

The control strategy is very simple. Each converter works as a current source. The higher solar irradiance is, the higher the stack current will be.

2.2.6   Summarized comparison of the studied architectures

The following table summarizes the characteristics of the studied architectures:

Architecture	MPPT efficiency	Power conversion efficiency	Volume	Weight	Architecture control complexity	Redundancy
DC to AC and AC to DC architecture	Bad	Low	High	High	High	No
Parallelized DC to AC and AC to DC architecture	Good	Low	High	High	Very high	No
DC to AC and AC to DC architecture with parallelized DC to DC	Good	Lowest	Highest	Highest	Very high	No
DC to DC architecture	Bad	Good	Lower	Lower	Low	No
Parallelized DC to DC architecture	Good	Good	Lower	Lower	Low	Yes

Usually, 50 Hz transformers or filters use to be big and heavy. The cost of the power stage is incremented with the filters cost, thereby cost is related with volume and weight.

ELY4OFF

2.2.7   Selected architecture for ELY4OFF project

Several figures of merit are identified and analyzed. This figures of merit are rated on each architecture. Finally, a comparison table shows that the best solution will be a parallelized DC to DC architecture.

3. Topology selection

3.1   Introduction

In the ELY4OFF project we must convert a high side DC bus (between 500V and 800V approximately) into a low side DC bus (between 110V to 165V approximately) achieving high efficiency (>90%) and galvanic isolation as desired requirement.

Along this deliverable, several topologies will be analyzed and one of them will be chosen.

3.2   Non-isolated DC/DC topologies

There are several non-isolated DC to DC topologies that can feed a low voltage side from a higher voltage. Some examples are buck, synchronous buck, Sepic, etc. All of them must switch the voltage on the high side and the current of the low side.

$$P_{in} = P_{out} + P_{losses} = V_{in} * I_{in} = V_{out} * I_{out} + P_{losses} \qquad (1)$$

$$P_{losses} = f(V_{in}, I_{out}) \qquad (2)$$

For the same power, lower the voltage in the low side, higher the current in the low side. If the voltage conversion ratio is higher than 4:1, which is our case, switched power is much higher than transferred power, leading to higher losses and lower efficiencies.

Besides, one desirable requirement is that in the case of an earth fault in one of the strings, the rest of strings should keep working. This is not possible if DC to DC converters are non isolated.

A transformer lets to adapt the voltage conversion and provides isolation.

3.3   Isolated DC/DC topologies

The aim of this section is to choose the best suitable and state-of-the-art topology with the most innovative semiconductors to be implemented within the ELY4OFF project.

A brief summary of most used industrial topologies is shown below.

3.3.1 Forward topology
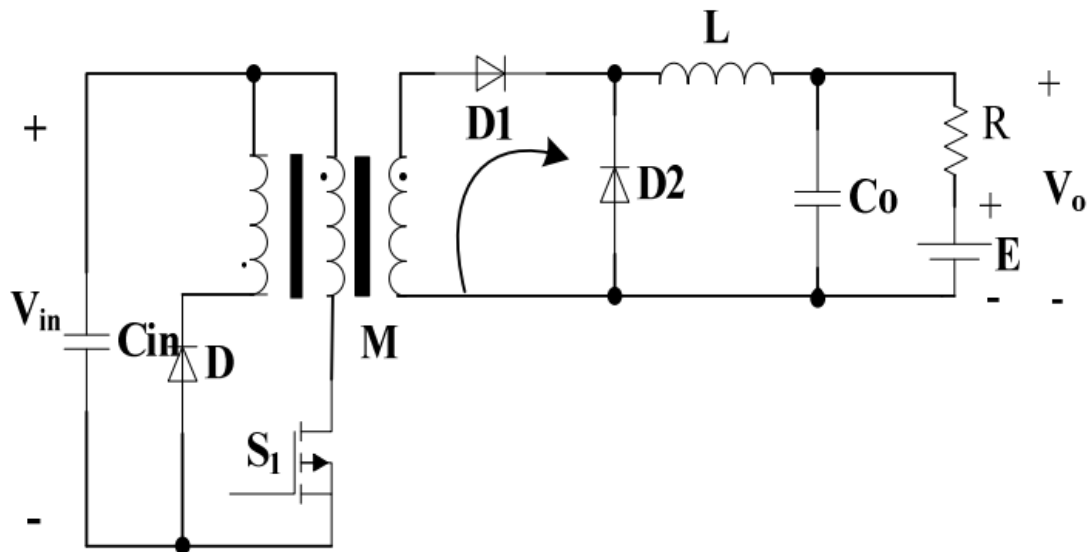
Fig. 7 Forward converter topology

The forward converter (Fig. 7) is a transformer isolated buck derived topology which can supply an output voltage either higher or lower than the input voltage.

On one hand, it requires a single ground referenced transistor and due to its non-pulsating output current, the rms content in the output capacitors is reduced.

On the other hand, it has small power capability (due to efficiency) and limited duty ratio because of the core reset. Besides, the drain voltage swings, at least, to twice the input voltage.

3.3.2 Flyback topology

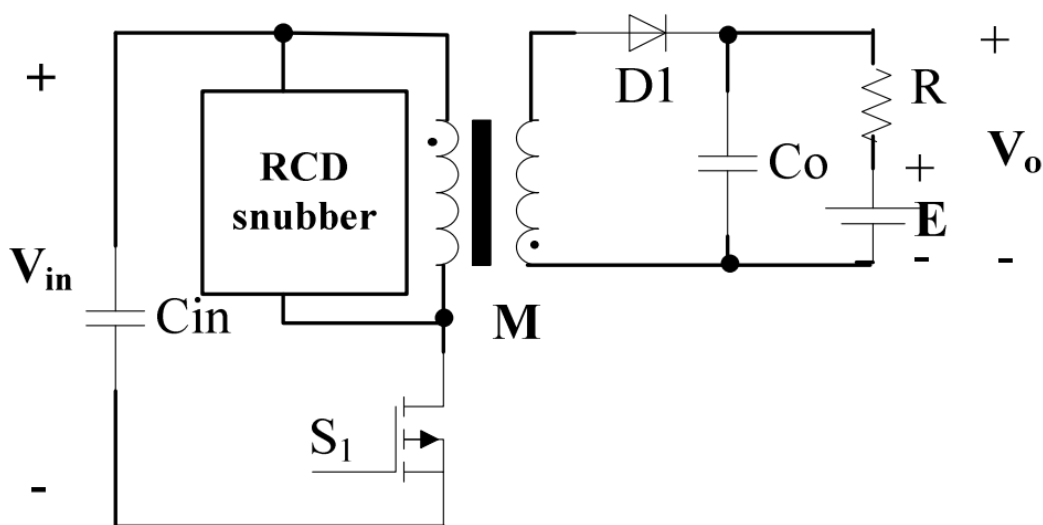*Fig. 8. Flyback converter topology*

The flyback converter (Fig. 8), is a transformer isolated buck-boost derived topology.

It requires a single ground referenced transistor and makes use of the magnetizing inductance of the transformer as the energy storage element.

Main advantages of this topology are a high efficiency for low power applications and the fact that non output filtering is needed, thus reducing the number of components to be used.

Nevertheless, as it operates at high switching frequency (above 100 kHz.), EMI/EMC filtering is mandatory and deserves due consideration.

Quite important is the output capacitor design, as it has to cope with a large value of ripple, resulting in the need of parallel capacitors in order to minimize power-losses.

3.3.3   Half-bridge topology
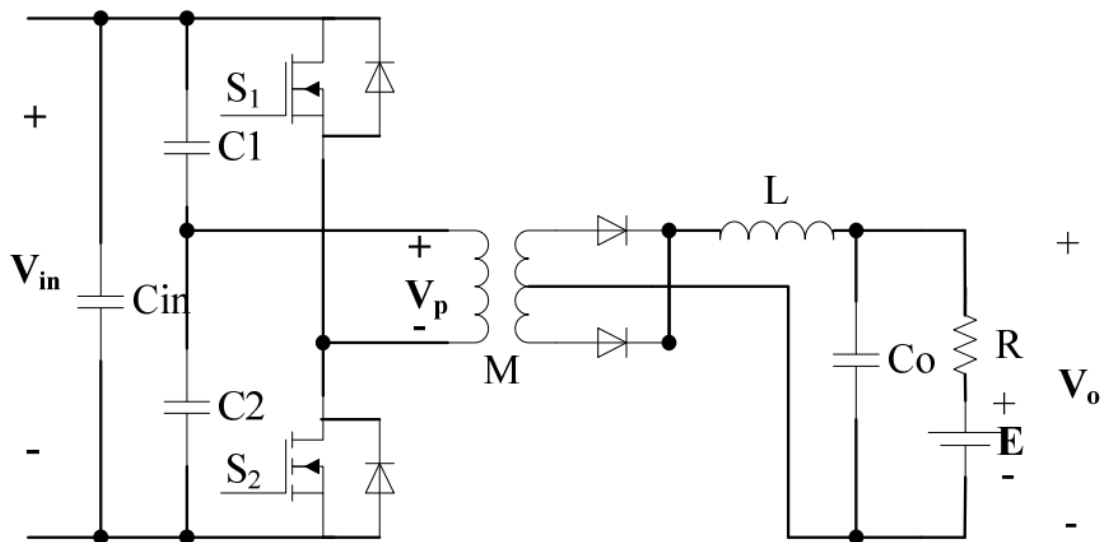
Fig. 9 Half-bridge topology

The half-bridge converter (Fig. 9) is a transformer isolated buck derived topology.

It requires two transistors and a centre-tapped secondary. It makes use the leakage inductance of the transformer as the intermediate energy storage element.

This topology exhibits lower input and output ripple currents compared with topologies with only one switching transistor and it is suitable for medium-power designs.

The control algorithm must include a capacitor voltage equalization strategy in such a way that the imbalance of the voltages of input capacitors is avoided.

3.3.4   Push-Pull topology
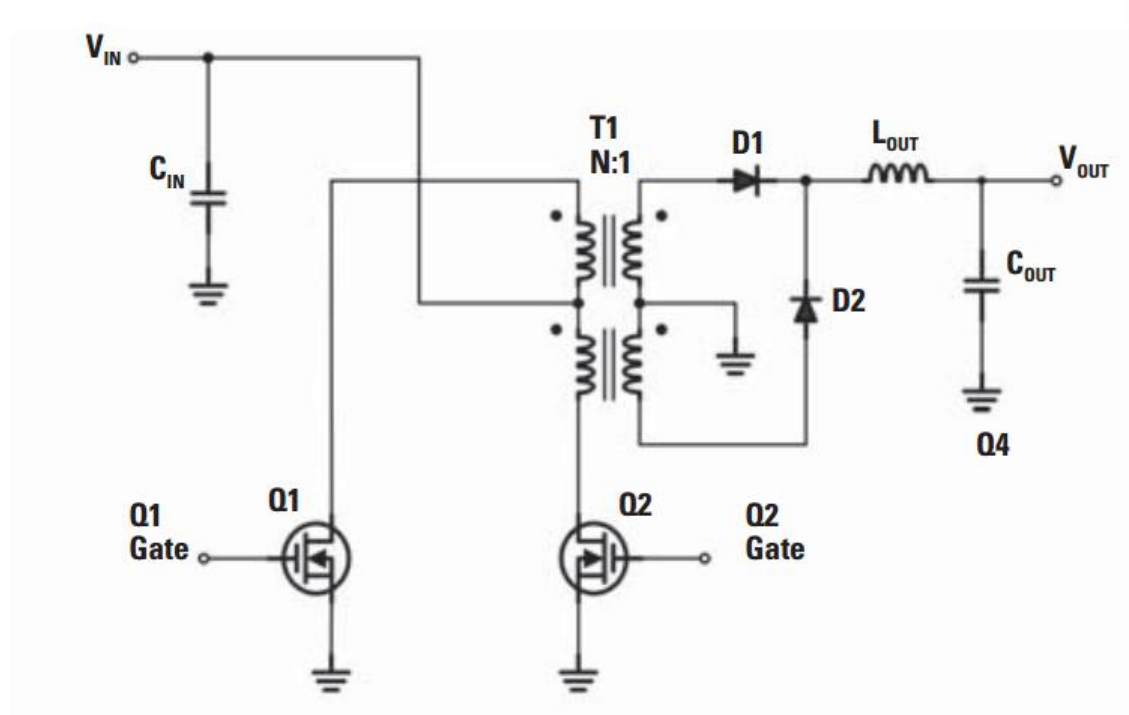
Fig. 10 Push-pull topology

The Push-Pull converter (Fig. 10) is a transformer isolated interleaved derived forward converter topology.

It requires two ground referenced transistors and a centre-tapped transformer, smaller than that of a forward converter. It uses the leakage inductance of the transformer as the component for energy transfer.

This topology is ideal for medium-power designs and has lower input and output ripple currents.

As this topology has typically flux imbalances in the transformer, magnetizing current is not reset to zero. Because of that the core flux can drift to saturation zones. A suitable control strategy should be used to deal with this behaviour.

3.3.5   Full-bridge topology

Fig. 11 Full-bridge topology

The full-bridge converter (Fig. 11) is a transformer isolated topology.

It consists of four power electronic transistors that form a full-bridge on the primary side of the transformer and a four-diode rectifier on the secondary side.

This topology allows the transistors to switch with zero voltage switching (ZVS) resulting in lower switching losses. It is ideal for medium to high power designs.

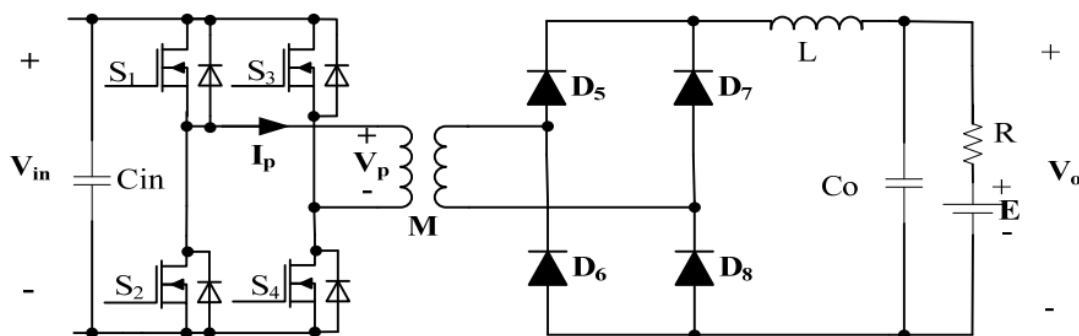In reference to the control of the converter, a microcontroller based one is recommended as there are various modes like voltage mode control (VMC), average current mode control (ACMC), peak current mode control (PCMC), etc.

3.3.6   Dual Active Bridge topology
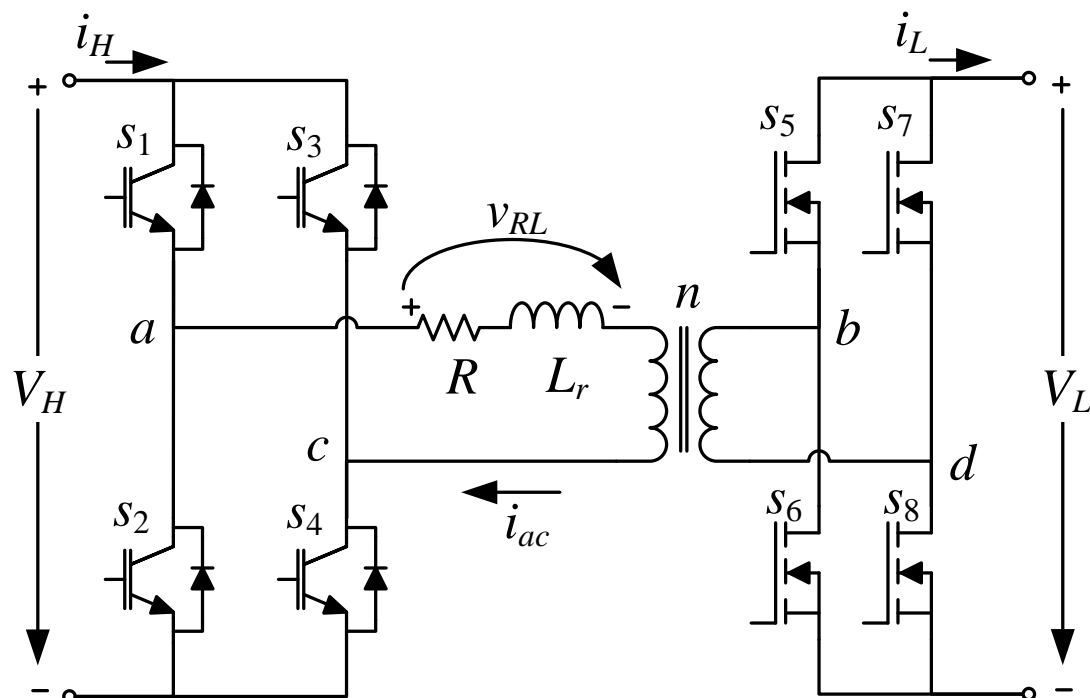
Fig. 12 Dual Active Bridge topology

The Dual Active Bridge converter (DAB) (Fig. 12) is a transformer isolated full-bridge derived topology.

It consists of eight power electronics transistors, four on the primary side and four on the secondary one.

This topology brings not only isolation and bi-directionality but also high performance and high efficiency because of its ZVS/ZCS switching behaviour in both sides.

High efficiency is restricted due to soft switching capability at light load conditions and high circulating current at heavy load conditions.

As voltage at transformer has a square wave form, there could be problems related to EMC/EMI.

3.3.7   Resonant Topologies

3.3.7.1   Full Bridge LLC topology
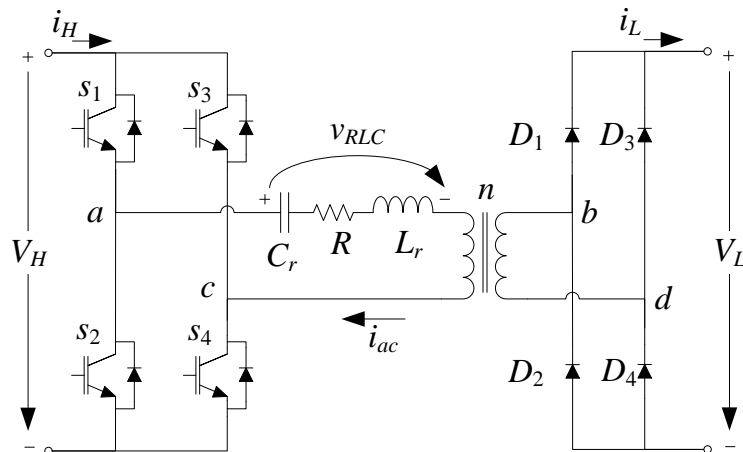
Fig. 13 Full Bridge LLC topology

The Full Bridge LLC converter (Fig. 13) is a transformer isolated resonant full-bridge derived topology.

It consists of four power electronic transistors in the primary side of the transformer, an inductor and capacitor for the resonant tank, a transformer and an output filter capacitor.

This kind of topology, as all resonant topologies, have several features such as high efficiency, and low EMI. It is unidirectional and designed for high power designs.

High efficiency is achieved due to Zero Voltage Switching (ZVS) working at high operating frequencies (in the hundreds of kilo Hertz).

However, regulation is not like conventional PWM schemes and a microcontroller is needed to define the best control strategy raising the control complexity of the converter.

Efficiency also can be compromised due to the output diodes as at high power designs and low output voltages, losses can be significant in comparison to the overall losses of the system.

3.3.7.2   Dual Active Bridge Series Resonant Converter topology (DAB-SRC)
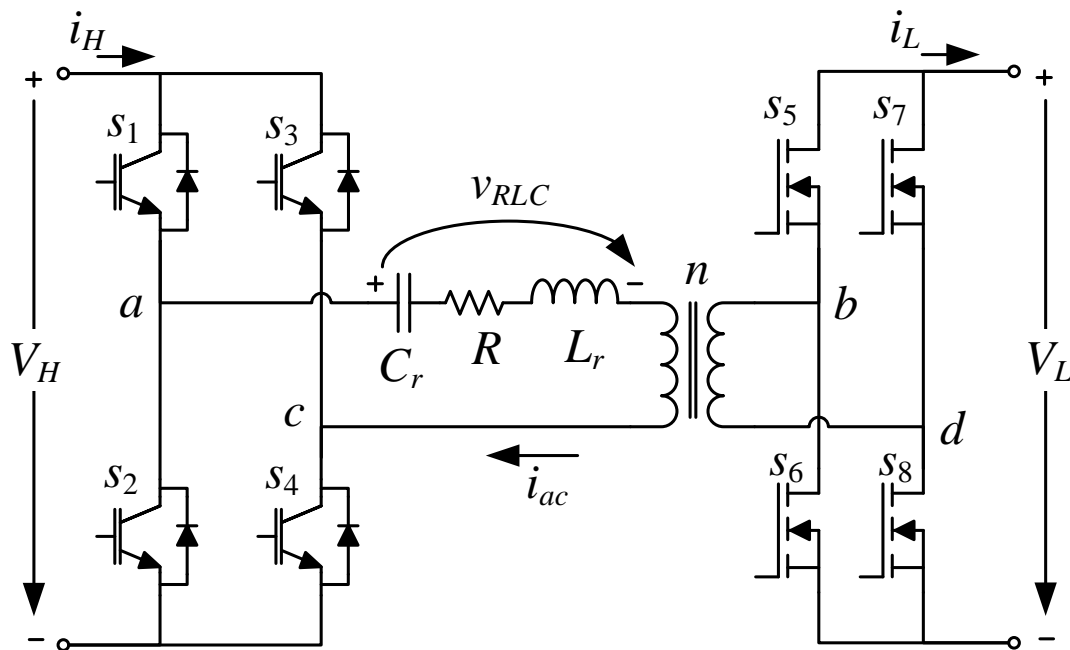

Fig. 14 Dual Active Bridge Series Resonant Converter Topology

The Dual Active Bridge Series Resonant Converter (DAB-SRC) is a transformer isolated resonant DAB derived topology.

It consists of eight power electronics transistors, four on the primary side and four on the secondary one plus a capacitor and inductor for the resonant tank. This topology suits well for high power conversions and very high input/output voltage fluctuations.

Thanks to the resonant behavior, current waveform is near sinusoidal reducing EMI effects and increasing the soft switching capability of the converter.

Opposite to the Full Bridge LLC topology, using active components in the secondary side helps to reduce losses in those devices.

Nonetheless, modulation techniques are more complex than in other resonant topologies; even so a very high efficiency can be achieved with the right control.

If a full wave modulation strategy is adopted the conversion concepts depicted by Fig. 13 and Fig. 14 are identical. Indeed, if output MOSFETs of Fig. 14 are not controlled they behave as simple diodes, offering the same operation as those of Fig. 13. The fact is that thanks to a very low on-state resistance R_{dson} at the MOSFETs, conduction losses are much lower than conduction losses in a diode. Thus, it is of interest to switch-on the output MOSFETs of Fig. 14 during the same period of time where the output diodes should be switched on. This switching strategy is the so-called synchronous rectification. Conduction losses using synchronous rectification are 53% lower than conduction losses with diodes.

Another advantage of the DAB-SRC of Fig. 14 is that output MOSFETs allows advanced modulation strategies such as the phase shift control, leading to a broader input-to-output voltage conversion ratio.

Additionally, thanks to the output MOSFETs, reverse energy conversion from the low-voltage side to the high-voltage side is possible. This ability can be useful in several scenarios: energizing the high-voltage side for initializing wind-generators, feeding of the DC-Bus of pump-drives, etc…

3.4   Comparative between topologies

Best way to compare topologies is the use of figures of merit covering devices stresses, power capabilities, efficiency, control complexity, EMC/EMI and cost.

The result of the analysis can be seen in the following table:

Topology	Devices Stress	Power	Efficiency	Control	EMC/EMI	Cost
Forward	High	< 1 kW	Very low	Easy	Bad	High
Flyback	High	< 1 kW	Low	Easy	Bad	Low
Half bridge	Medium	< 2 kW	Medium	Easy	Bad	High
Push pull	High	< 6 kW	Low	Easy	Bad	Medium
Full bridge	Low	< 6 kW	Medium-High	Easy	Medium	Medium
DAB	Low	< 6 kW	Medium-High	Medium	Medium	Medium-High
Full Bridge LLC	Low	< 6 kW	High	High	Good	High
DAB-SRC	Low	< 6 kW	Very High	High	Good	High

3.5   Chosen topology

The most suitable topology is a DAB-SRC converter as its efficiency is the best of all studied topologies and its devices are submitted to low stresses.

4. Efficiency improvement of a DC DC converter with broadly variable input to output voltage ratio using Silicon Carbide technology

4.1   Introduction

As it has been pointed out the series resonant dual active bridge (SRDAB) [8]-[11] is well suited for the required application. The SRDAB require an intermediate AC stage allowing the inclusion of a transformer that solves the input to output voltage gap problem [12], see Fig. 14.

If the input and output voltages are kept close to constant values the design of the converter is quite a straightforward task [13]-[15]. On the other hand, if one (or both) of input or output voltages suffers of large variations, as it happens in the case of this project, it becomes difficult to achieve efficiencies of 90% or more all along the operation voltage range.

SRDAB offers significant advantages over other topologies for high power density applications [16]. The primary advantage is zero voltage switching in a wide range of operation, which drastically improves efficiency. The case of the project under study is a challenging scenario with a broad range of possible voltages at the input and output ports.

The wide band-gap of SiC is greater than 3eV (about 3 times that of silicon). This provides higher breakdown electric field than conventional materials, Si or GaAs, indicating that the power devices made of SiC can withstand much higher voltage stress with much lower on-resistance. Meanwhile, the large band gap energy of SiC also results in a much higher temperature capability and higher radiation hardness. Furthermore, SiC has a higher thermal conductivity, which leads to important benefits for power dissipation, and higher power handling capability [17]. These features make SiC an interesting option to build high voltage MOSFETs with significantly lower conduction losses than the Si counterparts. Additionally, when compared with IGBT technology, SiC MOSFETs exhibits a much faster switching transient so the switching losses are drastically reduced. Hence, SiC MOSFETs are more promising to build high power converters with high power density. Although SiC materials have superior characteristics, the impact of SiC devices in systems must be carefully studied, given their higher cost.

As a result many reported researches have discussed the application characteristics of SiC switching devices, mostly SiC JFET and SiC BJT, and their impact on basic converters such as buck, boost, and the H-bridge rectifier. But there are considerably fewer reported studies based on SiC MOSFETs for isolated bidirectional converters (IBDCs). Preliminary research exposed in [13] evaluates the suitability of the SiC MOSFETs in DAB converters. In [13] the experimental all-SiC MOSFETs converter input and output voltages are 800V and 400V respectively. In [14], the application performances of IBDCs based on all-Si and all-SiC power devices are comparatively analysed and validated, being the converter input and output voltages 280V and 260~300V respectively. Reference [15] presents the switching performance of a 10A/15KV SiC MOSFET in a dual active half bridge converter, which its input and output voltage levels equal to 12KV and 400V respectively. As it can be observed the input to output voltage conversion ratio is, in all these cases, almost constant.

The optimum efficiency is achieved when, considering the transformer voltage conversion, the equivalent input to output voltage ratio equals unity. This happens when the transformer ratio

equals the overall input to output voltage conversion gain [18]. The mismatching of these values lead to a considerably higher rms currents in the inductor, the transformer, and the switches, which increases overall losses and reduces the efficiency. It is obvious that a good matching is only possible if input and output voltages are kept close to a constant value. Fig. 15 shows the equivalent input to output voltage conversion ratio for several references. In [13] and [15] the transformer and conversion ratios have the same value and in [14] the relation between them is in the range 0.9~1.1, all them close to the optimum matching.

Table 1 shows the equivalent input-to output voltage conversion ratios of the project. The normalized unity conversion ratio arises when the nominal stack voltage of 125V is feed by a nominal PV voltage of 570V. As it can be observed, our equivalent input to output voltage conversion ratio evolves from 0.62 to 1.5, a very large variation compared to the state of the art, see Fig. 15. Therefore the converter's operation characteristics vary drastically depending on the operation point, making the achievement of high efficiency t difficult.

Table 1 Equivalent Input-to-output voltage conversion ratio

PV voltage	Stack voltage	Equivalent conversion ratio
570 V	125 V	1
500 V	165 V	1.5
800 V	110 V	0.62
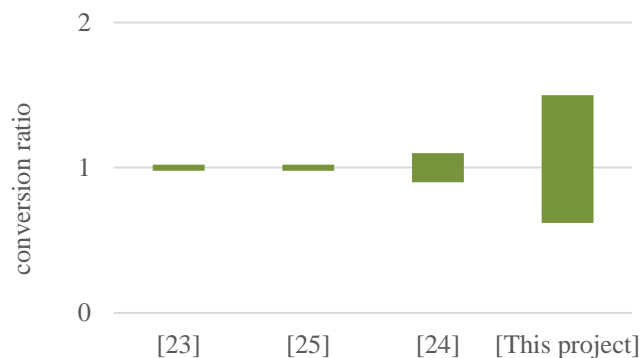
Fig. 15. Range of equivalent input to output voltage conversion ratio

4.2   Topology and operation principle

In the low voltage bridge silicon (Si) MOSFET technology is the obvious choice, since its switching time is much smaller than that of IGBT, and therefore its switching losses are smaller. But for the high voltage bridge Si MOSFETs cannot be employed due to the steep increase of their conduction resistance (Rds(on)) with blocking voltage. So that the high voltage side bridge utilizes IGBTs.

Fig. 16 shows the primary-side equivalent circuit of the SRDAB, where vac depicts the high voltage bridge output, on the left side of the resonant tank, n vbd is the low voltage bridge output on the right side of the resonant tank and vRLC and iac are the resulting resonant-tank voltage and current, respectively. Equivalent series resistance R takes into account several losses in the resonant tank.

Fig. 16. Simplified equivalent SRDAB circuit

Fig. 17 shows the evolution of the relevant variables when δ phase-shifting plus frequency control is used, which is the control strategy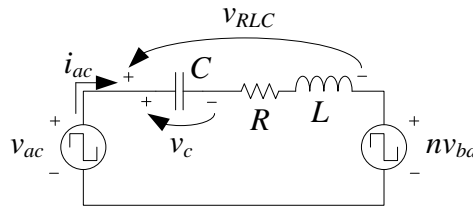 of the SRDAB of this work. The energy flows from the high voltage DC bus to the low-voltage side. The advantages of the resonant tank become evident when operating at high powers and close to the resonant frequency. In this situation a quasi-sinusoidal ac-link current is obtained, leading to reduced eddy current losses in windings and very low reactive power flow in the transformer. Active power flows from the leading bridge to the lagging one. The switching frequency is always above the resonant one and, as long as the phase of the current iac is kept between the phases of vac and nvbd voltages, lossless turn-on switching (zero voltage switching-ZVS) is assured in both IGBTs and MOSFET bridges at instants t1 and t4.

The turn-off strategy deserves a more thorough explanation. The ideal scenario should be that both IGBTs and MOSFETs are turned-off with a minimum current, thus minimizing switching losses. The fact is that due to the large input and output-voltage variability range it is not possible to achieve such an ideal case, so a suboptimal approach is retained. For a given exchanged power, currents at MOSFETs are always n times higher than currents at IGBTs, e.g. 45A versus 8A in the case of this project. Therefore the most judicious approach is to minimize the turn-off currents at MOSFETs. This can be achieved if the phase shift δ is chosen to be higher but close enough to t1 in such a way that low-current turn-off (ItoMOSFET) is assured, as shown in Fig. 17. The drawback is a high-current turn-off at IGBTs (ItoIGBT), which will be the major source of power losses in the converter. This is the core of the optimization strategy proposed for this work: first, thanks to an appropriate control strategy, the main losses are concentrated at IGBTs; second, IGBTs are replaced by SiC devices so that the overall efficiency is drastically improved.
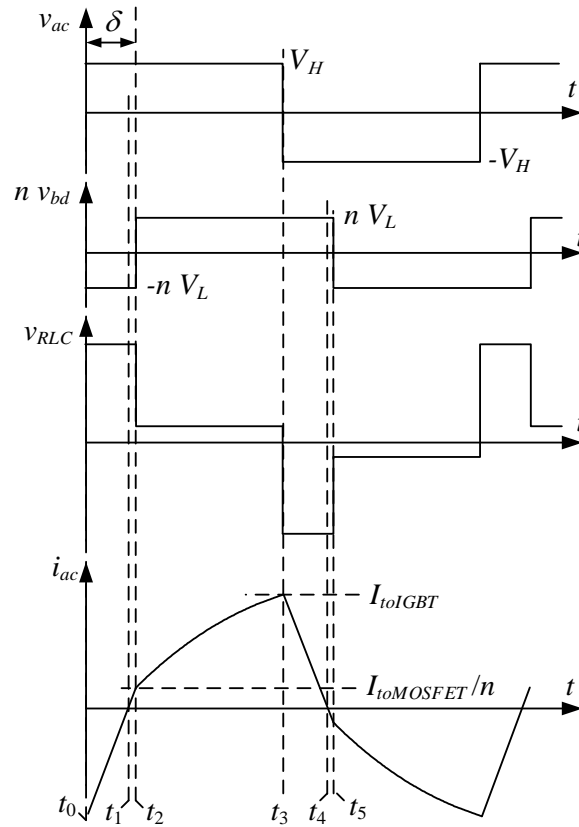
Fig. 17. Evolution of the main variables during a switching period

Table 2 summarizes hard switching (HS) and ZVS occurrences during the switching period of Fig. 17.

Table 2 Switching occurrences

time	High-Voltage Bridge		Low-Voltage Bridge	
	S1/S4	S2/S3	S5/S8	S6/S7
t_0	off	turn off HS	off	off
t_1	turn on ZVS	off	off	turn on ZVS
t_2	on	off	off	turn off HS
t_3	turn off HS	off	off	off
t_4	off	turn on ZVS	turn on ZVS	off
t_5	off	on	turn off HS	off

4.3   Turn-off energy model and estimation of converter's efficiency

On order to validate the proposed strategy two different designs have been compared, one of them using 1200V IGBTs by Infineon (IHW15T120) and the other one based on a 1200 SiC Z-

FET by Cree (CMF20120D). Both designs include a snubber capacitor across each device in order to slow down the voltage rise during turn-off transients. Thus, since the current fall will take place at lower voltage values, switching losses are reduced. Moreover, voltage spikes and electromagnetic interference (EMI) problems, associated with high dv/dt and stray inductances present in the circuit, are minimized. Given the difficulty to approximate switching losses from the data supplied by the manufacturer, an experimental test is performed with the purpose of modelling carefully the turn-off losses of the switches.

4.3.1   Turn-off energy model.

Table 3 shows the references and main characteristics of the tested devices. As the rms current at the resonant tank is always below 15A, SiC technology offers lower on-state conduction losses. If the rms current increases, the conduction losses of SiC technology equal or surpass those of Si-IGBT technology and, therefore, the improvement in overall losses is reduced.

Table 3 Devices under test

Ref.	IHW15T120	CMF20120D
Manufacturer	Infineon	Cree
Techn-nology	Si IGBT	SiC Z-FET
V_{max}	1200V	1200V
I_{DS}	30A@25ºC	42A@20ºC
Q_g	85nC	91nC
ON-state V_{ce}/V_{ds} @10A	1.5V @150ºC	1V @135ºC
ON-state V_{ce}/V_{ds} @15A	2.1V @150ºC	1.6V @135ºC

Fig. 18 shows the test circuit with the H-bridge, built up by the devices under test (DUT), and an inductive load. The switching conditions are the same as in the application, i.e. the current lags voltage and the diode turns on before the transistor does. As shown in Fig. 18 the gate to source voltage (vGS), drain to source voltage (vDS) and drain current (iDS) are measured. Fig. 19 depicts the resulting turn-off waveforms at VH=600V and IDS=6A. The speed of switching can be easily characterized by the current fall time. As expected the SiC Z-FET (Fig. 19.b), with a fall time of 110ns is faster than the IGBT technology (Fig. 19.a), which needs up to 650ns to turn-off. It has to be noted that, though the behaviour of drain to source voltage of the SiC MOSFET shows a ringing, its overshoot is lower than that of the IGBT technology.
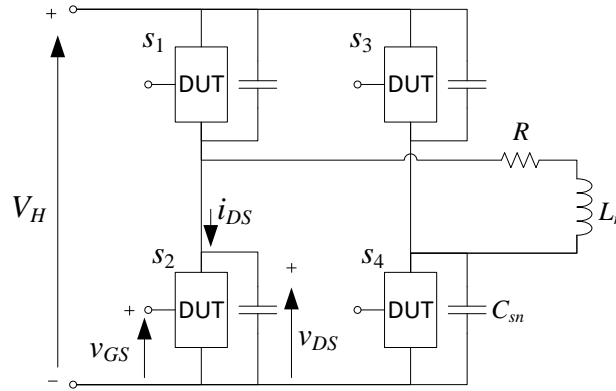
Fig. 18. Switching performance test circuit.

a)   b)
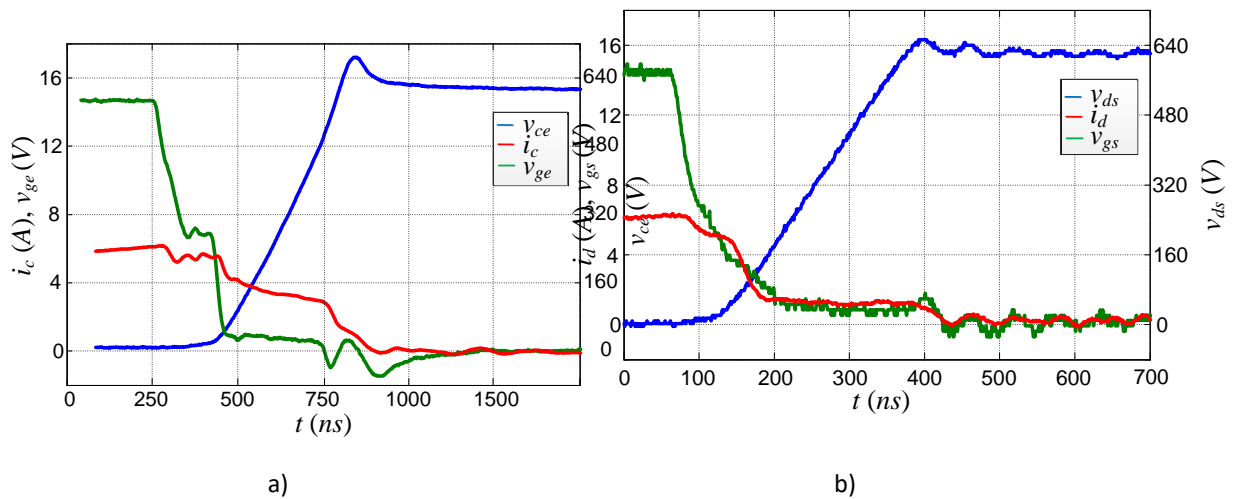
Fig. 19. Turn-off waveforms at VDC=600V and IDS=6A: a) IGBT, b) SiC Z-FET

Following the same procedure a large set of tests has been carried out considering different turn-off currents. This way the experimental turn-off energy Eoff of each point of operation has been measured. Approximate polynomials have been obtained using standard curve-fitting techniques. Equations (3) and (4) show the polynomials for IGBT and SiC technologies under Vds=600V, being Ito the turn-off current.

$$E_{off(IGBT)}[\mu J] = 4.68I_{to}^2 - 17.01I_{to} + 261.5 \quad (3)$$

$$E_{off(SiC)}[\mu J] = 7.362I_{to} + 66.93 \quad (4)$$

Fig. 20 shows the measured and approximate turn-off energy values.

Fig. 20. Measured and approximate turn-off losses for V_{ds}=600V

4.3.2   Estimation of the power losses at the switching devices under different operating conditions.

Any operation point is defined by the power to be transferred, P, and the voltage values of the interconnected ports, VH and VL. The control algorithm follows the principles explained in section II. It selects the switching frequency fsw and the phase shift δ assuring that a) the phase of the low voltage bridge output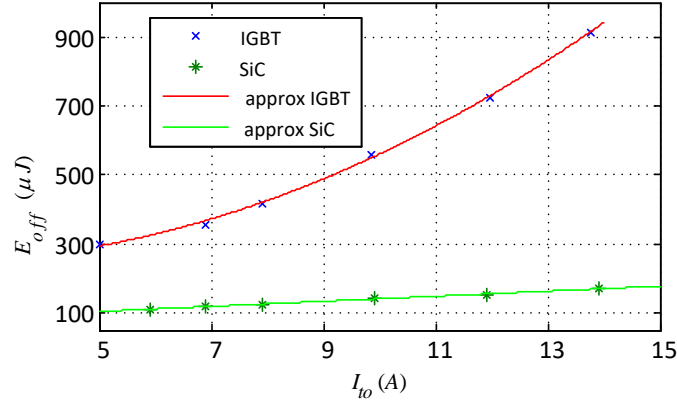 vbd is aligned with that of the resonant current iac, and b) the amplitude of the resonant current iac is the required one in order to get the desired power P to exchange.

The losses estimator takes into account each operating point and, using the state-space model, computes the rms and switch-off currents at each device. Turn-off energy loss per device Eoff during a switching period can be computed using equation (3) for IGBTs or equation (4) for SiC technology. The overall switching losses per device P_{sw} can be computed by equation (5).

$$P_{sw} = f_{sw}\, E_{off} \qquad (5)$$

IGBT's conduction losses $P_{on(IGBT)}$ are the addition of diode and transistor conduction losses, as shown in equation (6). $\langle I_{IGBT}\rangle_{avg}$, $\langle I_{Diode}\rangle_{avg}$ and $\langle I_{Diode}\rangle_{avg}$ are computed for each operating point by analytic formulae obtained from state-space models.

$$P_{on(IGBT)} = \langle V_{ce}\rangle_{sat}\, \langle I_{IGBT}\rangle_{avg} + V_f\, \langle I_{Diode}\rangle_{avg} \qquad (6)$$

Contrary to IGBT's, if the SiC MOSFET is turned-on it allows reverse conduction through the channel. Because of that the current flows across the antiparallel diode only during dead-time periods, which are negligible. So SiC MOSFET conduction losses can be computed by equation (7), where $\langle I_{MOSFET}\rangle_{rms}$ and $\langle I_{Diode}\rangle_{rms}$ are also analytically computed at each operation point.

$$P_{on(MOSFET)} = R_{DSon}\langle I_{MOSFET}\rangle_{rms}^2 \qquad (7)$$
$$+ R_{DSon}\langle I_{Diode}\rangle_{rms}^2$$

4.4   Efficiency improvement

Using the above mentioned losses model it is possible to compute the improvement of power losses achieved by SiC technology under different operating conditions. Four stack voltages are studied (115V, 130V, 145V and 160V) and three power exchange levels are analysed (1200W, 2000W and 3600W). High side voltage is kept at 600V. Table 4 shows the computed improvement of power losses in each case. The 115V/3600W case falls out of the operation range due to control mapping limitations.

Table 4 Estimated improvement of losses

Vucap (V)	ΔP (W)@1200W	ΔP (W)@2000W	ΔP (W)@3600W
115	63.1	84.5	-
130	56.6	66.5	99.9
145	53.3	54.2	73.1
160	52	43.3	50.5

There are two main parameters to be considered when analysing switching losses: turn-off current and switching frequency. In the SRDAB of this project, switching frequency depends on the converted power and does not change with the voltage level at the stack. The higher the power, the lower the switching frequency. On the other hand, the turn-off current increases when the power increases and when the voltage level at the stack decreases. So the best opportunities for power losses improvement are located at low voltage levels and high power values, as observed at Table 4.
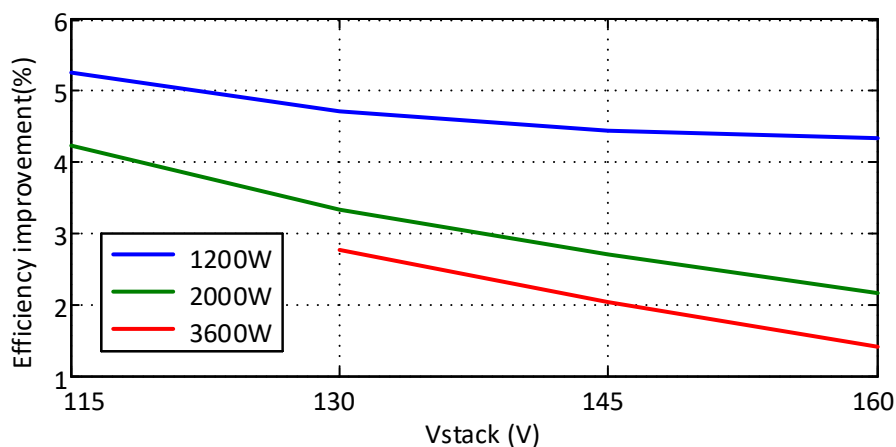
Fig. 21 shows the estimated efficiency improvement percentage based on data from Table 4.
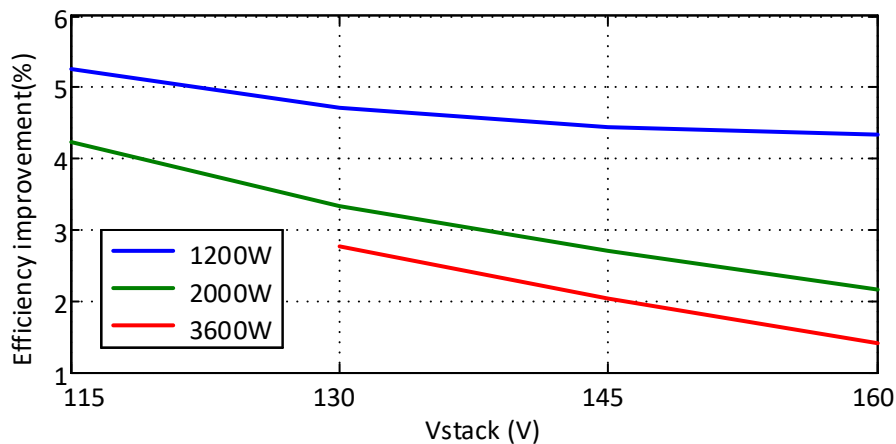

Fig. 21. Estimated improvement of the efficiency

¡Error! No se encuentra el origen de la referencia. shows estimated efficiencies using IGBTs (solid lines) and SiC devices (dashed lines). As it can be observed, thanks to the proposed control strategy combined with the SiC technology satisfactory efficiencies over 90% are obtained along all the operating range, or over 94% if only 1.2kW is converted.

Supposing an ambient temperature of 45ºC and a maximum allowable case-temperature of 70ºC the maximum admissible temperature gradient is 25ºC. Thanks to its lower power losses, the SiC technology allows non-stop permanent nominal operation whereas the IGBT-based converter should be switched off after 100 seconds of operation.

These figures can be still improved if lower conduction losses are achieved at the low side bridge. This can be easily assured if lower Rdson is obtained by using two parallelized mosfets in the position of each switching element.

4.5 Conclusion

It is well known that SiC devices offer lower power losses than IGBT devices in some operation modes and ranges. So a simple IGBT-SiC replacement can improve the efficiency of the converter. Anyway the impact of this advantage can be boosted if the design of the converter considers, in an a-priori basis, the use of SiC devices. Instead of balancing the power losses between the high-side IGBT and the low-side MOSFET devices, the control strategy seeks for minimum switching losses at MOSFETs and concentrates the switching stress at IGBTs. Thus, the impact of the inclusion of SiC devices is magnified. The new DC/DC converter achieves efficiencies over 90% along almost all the operating range. The combination of the control strategy and the SiC devices leads to the possibility of non-stop permanent operation, which was not possible for an IGBT-based converter. Further efficiency improvement is still possible if two or more mosfets are parallelized.

5. Overarching C&CS: Communication protocols and signals for interaction with PEMWE, PV generation and HSS

The overarching C&CS has to coordinate the operation of the equipment deployed in ELY4OFF. The following figure shows the devices to be controlled (those reached by red arrows):
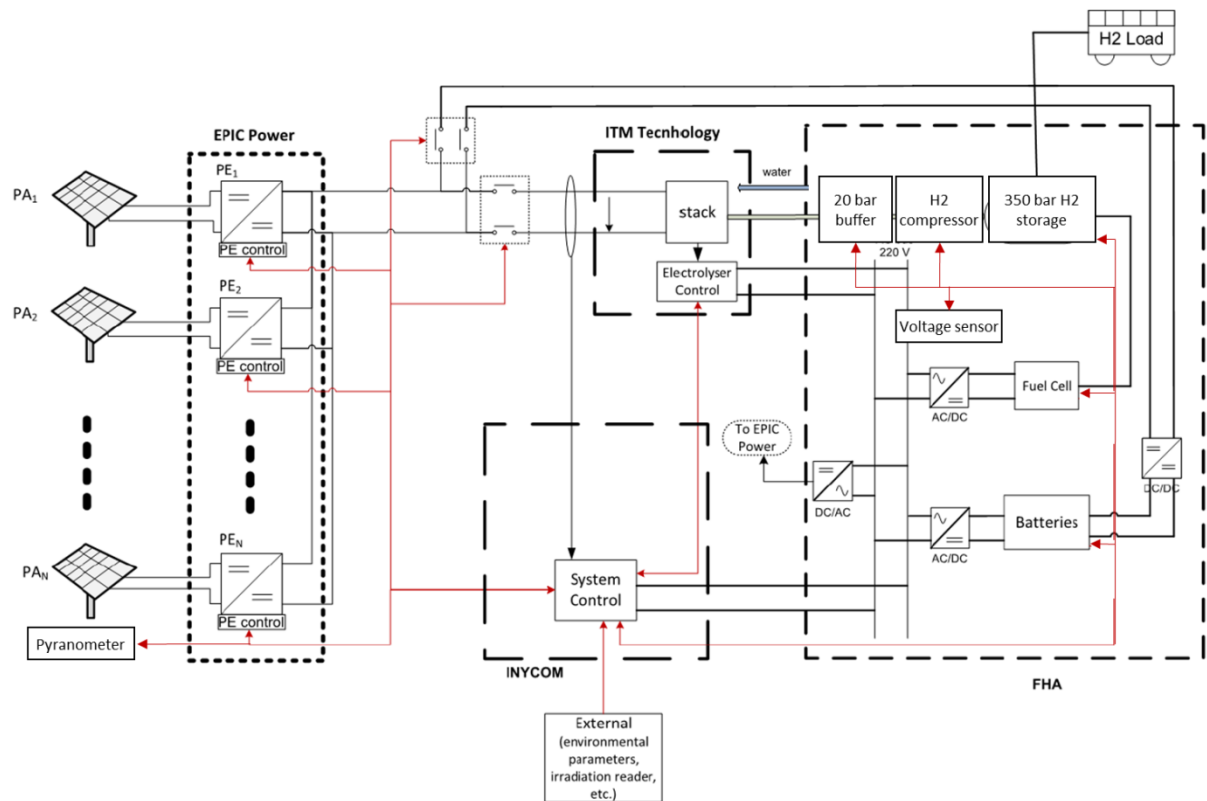
Fig. 22. Elements to be controlled by the overarching C&CS developed by INYCOM.

5.1   PEM water electrolyser (PEMWE)

A description of the PEMWE provided by ITM has been provided in previous deliverables.

5.1.1   Signals transmitted from the overarching C&CS to the PEMWE C&CS

The overarching C&CS will send to the PEMWE PLC the following command data based on previous analysis, management and decision making, considering the information gathered by the sensors and equipment installed:

- Plant run command (start/stop). On/off command to the PEMWE in order to cut off/ or start the hydrogen production.
- Input current. Current setpoint at which the PEMWE should operate in order to maximize the hydrogen production, assuring that other technical and safety requirements are covered.
- Buffer tank pressure. Availability of hydrogen storage to be taken into account by the PEMWE C&CS.
- Communications heartbeat (1Hz=healthy). This will be 1 Hz signal from the overall DCS system which will tell our system that DCS system is still up and running

- Plant run command (1=run, 0=shutdown). Send the Plant into Generation once all the initial checks are done
- Full Capacity During Day (day mode). Signal to indicate that there is enough Power Available to send the Plant in Generation
- Essential Capacity During Night (Night mode). Signal to indicate that there is not enough Power Available to send the Plant in Generation only essential services will Run
- Standby Mode (if power is below threshold or signal from control system)
- Acknowledge alarms (1=ack) - Acknowledge any alarms. Plant will not go into Generation if there are any active alarms
- [Optional]: Demand %. Determine the Production Rate of the Plant.

In principle, the standby mode is meant for periods when the electrolyser is in operation but the power delivered by the DC/DC converter is below a certain threshold but it is not desired to enter yet to the Night mode.

5.1.2   Signals sent from the PEMWE C&CS to the overarching C&CS

The overarching C&CS will receive information from PEMWE operational status at different levels for analysis, management and decision taking. The overarching C&CS must be aware of any warning or alarm that might occur in the PEMWE subsystem so that if there is any inconvenient, the overarching C&CS can stop the feed of solar energy to the electrolyzer and use it to charge the batteries. The signals the overarching C&CS can read are listed below:

- Communications heartbeat
- Plant health signal
- Copy of run command
- E-stop activated
- Shutdown 1
- Shutdown 2
- Smoke detector tripped
- PSU fault
- PSU status
- Plant operator override
- Plant status
- Plant power (kW)
- Plant energy counter (kWh)
- Dew point reading
- H2 in air
- Plant demand (%)
- Plant output (%)
- Dryer output temperature (^{o}C)
- Control room temperature
- Stack compartment temperature

Additionally all this information gathered by the overarching C&CS (alarms, instrumentation values, operating state…) will be shown in its SCADA to have a quick view of the status of the

electrolyser and its current setpoint. Thus, the HMI of the PEMWE C&CS will be sent via Profinet to the overarching C&CS.

5.1.3 Communication protocol and connection between overarching C&CS and PEMWE C&CS

The communication protocol used to exchange information between the overarching C&CS and the PEMWE PLC will be Profinet. Profinet is an industry technical standard for data communication over Industrial Ethernet (TCP/IP) able to deliver data under tight time constraints (on the order of 1ms or less) and its supported by most of the industrial PLCs in the market.

All network connections should be made using 4-core Profinet cable with ruggedized RJ45 connections.

5.2 Photovotaic (PV) panels

The PV will send radiation information through a pyranometer installed by FHA[1]. The pyranometer will send a radiation through a 4…20 mA current signal previously amplified and converted.

5.3 Power electronics (PE)

The power electronics include, in this document, the DC/DC converter to accommodate power from the PV to the PEMWE. The remaining low power converters (DC/AC inverters from battery and fuel cell to the AC bus, and the AC/DC rectifier from AC bus to DC/DC converter) are considered in the scope of the hybrid storage system built by FHA (see section 5.4).

5.3.1 Signals transmitted from the overarching C&CS to the PE C&CS

The following signals will be transmitted from the overarching C&CS to the PE C&CS to act on them:

Variable name	Start bit	Bit length	Scaling	Type	Description
EN_SM	0	1	NA	Unsigned	0 = Conversion disabled 1 = Enable conversion to feed the stack
EN_VM	1	1	NA	Unsigned	0 = Conversion disabled 1 = Enable conversion in voltage mode
I_MAX	16	16	0.1A/1	Unsigned	Maximum output current (0 to 1000.0 A)

Table 5. Signals transmitted from the overarching C&CS to the PE C&CS.

5.3.2 Signals sent from the PE C&CS to the overarching C&CS

The overarching C&CS will receive input information from the PE for further analysis and decision taking. The signals received are summarized in the following table:

Variable name	Start bit	Bit length	Scaling	Type	Description

---

[1] http://www.alphaomega-electronics.com/en/radiacion-solar/835-piranometro-lp-pyra-03-de-radiacion-solar-global.html

V_HS_nn	0	16	0.1V/1	Unsigned	Input voltage (0.0 to 1000.0 V)
V_LS_nn	16	16	0.01V/1	Unsigned	Output voltage (0.00 to 180.00 V)
I_HS_nn	40	8	0.1A/1	Unsigned	Input current (0.0 to 20.0 A)
I_LS_nn	32	16	0.1A/1	Unsigned	Output current (0.0 to 100.0 A)
Tamb_nn	48	8	1ºC/1	Signed	Operating temperature (-50 to 127 ºC)
THS_nn	0	8	1ºC/1	Signed	Internal temperature 1 (-50 to 127 ºC)
TLS_nn	8	8	1ºC/1	Signed	Internal temperature 2 (-50 to 127 ºC)
Status_nn	16	8	NA	Unsigned	DCDC converter state (0 to 255)
Warning_nn	24	8	NA	Unsigned	(0 to 255) 0 = No warning 1 = High temperature
Error_nn	32	8	NA	Unsigned	(0 to 255) 0 = No error 1 = DC link voltage error detected (voltage over 900 V) 2 = Stack voltage error detected 3 = DC link overcurrent detected (over 11 A) 4 = Stack current error detected 5 = Reserved 6 = Overtemperature error (internal temperature over 80ºC) 7 = Error when stack side is switched ON 8 = Reserved 9 = Internal error 1 10 = Internal error 2
*nn is the number of converter from 01 to 13					

Table 6. Signals sent from the PEMWE C&CS to the overarching C&CS.

5.3.3   Communication protocol and connection between overarching C&CS and PE C&CS

The overarching C&CS will be connected via CAN 2.0B, which requires:

- Compatible hardware
- 125 kbps
- Extended identifiers (29 bits)

An isolator is needed as P2S CAN is earth grounded

5.4   Hybrid Storage System (HSS)

This subsystem is the responsible for storing hydrogen and supplying energy in moments of a low PV generation to all peripherals, for supplying hydrogen to the final application and for providing water to the electrolyser.

It consists of a hydrogen storage (composed by a low-pressure and a high-pressure tank), electrochemical batteries, a fuel cell and the associated electronics for charge and discharge. Its main purpose is to guarantee the source of energy to all the auxiliary equipment of the electrolyser as well as to the overarching C&CS, which has to be always in operation.

5.4.1 Electrochemical batteries

The lead-acid batteries selected by FHA for this application[2] are specially designed for Renewable Energy Storage applications which require regular deep cycling. A battery management system (BMS) will be installed with the batteries to manage the charge of the cells and its voltage. Therefore, the overarching C&CS will communicate with the BMS to exchange relevant information for the operation.

Signals transmitted from the overarching C&CS to the battery controller

- Enable/Disable Charge
- Enable/Disable Output

Signals sent from the battery controller to the overarching C&CS

- State of charge (SoC)
- Error codes
- System pack balance

It is vital for the overarching C&CS to have information about the SoC of the batteries, because depending on the battery level the C&CS will have to prioritize the Hydrogen production or the charge of the batteries in order to have enough energy supply for all the auxiliary equipment.

Communication protocol and connection between overarching C&CS and battery controller

An industrial communication protocol, such as CAN or Modbus TCP, will be used to exchange information between the BMS and the overarching C&CS and the final decision will depend on the BMS installed and its possibilities of communication.

5.4.2 Fuel cell (FC)

The fuel cell installed at FHA facilities[3] is going to be used to keep the electrolyser operational and complement the operation of the lead-acid batteries. The strategy is to operate the fuel cell when the lead-acid batteries are in low SOC and there is not sufficient radiation.

Signals transmitted from the overarching C&CS to the FC C&CS

- Start/stop operation

Signals sent from the FC C&CS to the overarching C&CS

- Operational: yes/no

Communication protocol and connection between overarching C&CS and FC C&CS

CAN Bus v2.0A (Standard 11 bit), Baud Rate 250 kbit/s

---

[2] http://www.technosun.com/es/descargas/SUNLIGHT-RES-OPzS-ficha-EN.pdf
[3] HyPM HD 4-200 PN model of Hydrogenics

5.4.3   Hydrogen storage (HS)

It consists of a low-pressure H2 tank and a high-pressure H2 tank[4], both of them provided with a pressure sensor to estimate the hydrogen availability in the system.

Signals transmitted from the overarching C&CS to the HS

The overarching C&CS does not send setpoints to the HS. Both the PEMWE and the compressor deliver hydrogen to the low and high pressure tanks when requested.

Signals sent from the HS to the overarching C&CS

Pressure value in both tanks

Communication protocol and connection between overarching C&CS and HS

Both pressure sensors have an analog signal of 4-20 mA that will be wired directly to the PLC of the overarching C&CS.

5.4.4   Hydrogen compressor (HC)

The hydrogen compressor[5] is currently being automated by FHA to control the different valves and instrumentation. The overarching C&CS will send/receive the following information:

Signals transmitted from the overarching C&CS to the HC

Start/stop command

Signals sent from the HC to the overarching C&CS

In principle, FHA may send the status (operational/not operational) to the overarching C&CS, but FHA is in charge of controlling the HC.

Communication protocol and connection between overarching C&CS and HC

Digital signal representing the start/stop command[6].

5.4.5   Voltage meter (VM) at 220 V AC bus

FHA is planning to introduce a voltage meter to verify that the 220 V AC bus is ready to deliver power to the PEMWE.

Signals transmitted from the overarching C&CS to the voltage sensor

Not applicable.

Signals sent from the voltage sensor to the overarching C&CS:

---

[4] High pressure: 350 bar; low pressure: 20 bar (being agreed between ITM and FHA)
[5] http://www.thomasnet.com/catalogs/item/235111-4460-1001-1054/haskel-international/model-agt-8-inch-in-series-two-stage-pneumatic-driven-gas-booster/
[6] Automation of the HC C&CS in progress. Digital signal is suitable for an Arduino C&CS.

Voltage value

Communication protocol and connection between overarching C&CS and voltage sensor

Modbus protocol[7]

5.4.6   Power converters around the 220 V AC bus

Initially, the following power converters at FHA do not need to be controlled, as they enter into operation as soon as detecting input voltage:

- DC/AC inverter (from FC to 220 V AC bus)
- DC/AC inverter (from battery to 220 V AC bus)
- AC/DC rectifier (from AC bus to DC/DC converter)

---

[7] Tentative, as most of power quality analyzers use this protocol.

6. Overarching C&CS: hardware requirements

Based on the analysis of the signals to be transmitted and received by the overarching C&CS the chosen hardware should have the following features:

- Support for PROFINET, Modbus and TCP protocols.
- Flexibility to incorporate different analog and digital I/O modules.
- Ethernet connection
- DB connectivity
- Webserver for HMI development

A Phoenix Contact PLC controller has been selected due to the following reasons:

- Standard language availability (IEC 61131-3).
- Commercial availability and line-up: there is a comprehensive line-up that easily allows scaling the control system from a very small and cheap solution.
- Support for PROFINET and Modbus TCP. Availability of modules to incorporate CAN protocol.
- Availability of a web server for the design of a HMI.

The hardware selected for this application based on the signals defined on the previous section is:

Component	Technical features
Phoenix Contact ILC 191 ETH 2TX	1.3 ms 1 K mix instructions 1 MB RAM Program memory (1 MB each) SD card 2 Ethernet connectors Maximum 4096 IO points PROFINET device Modbus TCP Server and Client WebServer for HMI development Supported protocols: PROFINET, HTTP, FTP, SNTP, SMTP, SQL, MySQL 8 Digital Inputs 4 Digital Outputs
IB IL CAN-MA-PAC	Master CAN Inline. Transmission speed: 1Mbps (maximum). Maximum data width (128bytes)
IB IL 24 DO 8-PAC	8 Digital Outputs. 24V DC, 500 mA.
IB IL AI 8/SF-PAC	8 Analog Inputs (0-20 mA, 4-20 mA, ± 20mA, 0-10V,±10V). Two-wire connection.

Table 7 – PLC modules

*The I/O modules chosen could be changed depending on the final sensors and equipment installed at IHT facilities. Fig. 23 shows the PLC structured of the chosen PLC.
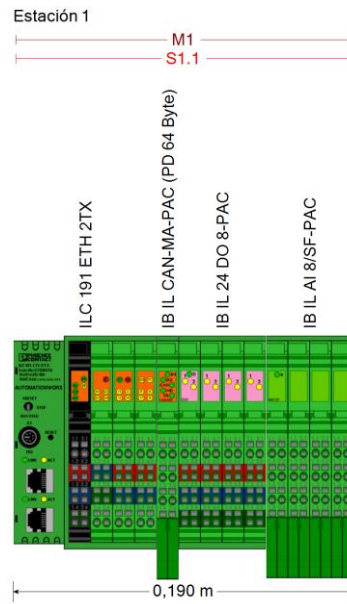
Fig. 23. PLC Structure

Additionally, a computer with an UPS, to monitor the system and to avoid a sudden loss of control, will be installed. The computer will be used to store the data acquired by the sensors in a database and to access to the HMI of the overarching C&CS to monitor and control the system information and its subsystems (i.e, sun radiation, status of the system, SoC of the batteries, hydrogen storage, etc.). Moreover, the computer would allow the system to communicate with external weather stations via Internet (if available) to get weather information and will run predictive algorithms based on the information gathered to anticipate to any minor boundary condition modification (load changes, level of hydrogen storage, batteries). If the connection between the PLC and the computer is not available, it won't endanger the safe operation of the system, and the PLC will store the data collected locally until the connection is restored.

7. Conclusions

This deliverable has provided a status of the progress made in the design of subsystems for offgrid integration, which covers power electronics (DC/DC converter) and overarching C&CS. This progress is linked to the advances done in tasks 4.1 and 4.2 of ELY4OFF.

The main outcomes are listed below:

- For the DC/DC converter's architecture, the best solution will be a parallelized DC to DC architecture. For the selection, MPPT efficiency, power conversion efficiency, volume, weight, control complexity and redundancy criteria have been considered.
- The most suitable topology for the DC/DC converter is a DAB-SRC converter as its efficiency is the best of all studied topologies and its devices are submitted to low stresses. The advantages are also the suitability of power for the application and the EMC/EMI behavior while the drawbacks are a more difficult controllability and the costs.
- For achieving a high efficiency DC/DC converter, a simple IGBT-SiC replacement can improve the efficiency of the converter. Anyway the impact of this advantage can be boosted if the design of the converter considers, in an a-priori basis, the use of SiC devices. Instead of balancing the power losses between the high-side IGBT and the low-side MOSFET devices, the control strategy seeks for minimum switching losses at MOSFETs and concentrates the switching stress at IGBTs. Thus, the impact of the inclusion of SiC devices is magnified. The new DC/DC converter achieves efficiencies over 90% along almost all the operating range. The combination of the control strategy and the SiC devices leads to the possibility of non-stop permanent operation, which was not possible for an IGBT-based converter. Further efficiency improvement is still possible if two or more mosfets are parallelized.
- Regarding the overarching control and communication system, the specific signals to received/sent to the PEMWE, PE, PV and HSS components are clarified and agreed between partners.
- The communication protocols are also clear and minimum variations are expected.
- The overarching C&CS required hardware has been designed

The following next steps will be taken at this moment to continue the work started with this deliverable contributing to deliverables 4.4 and 4.5:

- Design, engineering and manufacturing of the DC/DC converter by EPIC Power for its installation in FHA facilities as part of deliverable D4.4. Deadline: month 23.
- Agreement in the control logic, software programming (considering the signals received/sent, the control logic as well as wheather forecasting algorithms), hardware ordering and installation in FHA facilities as part of deliverable 4.5. Deadline: month 23.

References

[1] European Council, EUCO 169/14 (23 and 24 October 2014) conclusions

[2] HyUnder project, Grant Agreement No. 303417, "Assessment of the Potential, the Actors and Relevant Business Cases for Large Scale and Long Term Storage of Renewable Electricity by Hydrogen Underground Storage in Europe. Executive Summary", 23th June 2014.

[3] e4Tech Sarl, Element Energy Ltd, "Development of Water Electrolysis in the European Union", Fuel cells and hydrogen Joint undertaking, February 2014.

[4] Solmecke H, Just O, Hackstein D. Comparison of solar hydrogen systems with and without power electronic DC/DC converters. Renew Energy Jan-Feb 2000;19(1e2):333e8

[5] Maeda T, Ito H, Hasegawa Y, Zhou Z, Ishida M. Study on control method of the stand-alone direct-coupling photovoltaic e water electrolyzer. Int J Hydrogen Energy March 2012;37(6):4819e28.

[6] Paul B, Andrews J. Optimal coupling of PV arrays to PEM electrolysers in solarehydrogen systems for remote area power supply. Int J Hydrogen Energy, Jan 2008;33(2):490e8

[7] Garrigos A, Blanes JM, Rubiato J, Avila E, García CG, Lizan JL. Direct coupling photovoltaic power regulator for stand-alone power systems with hydrogen generation. Int J Hydrogen Energy Oct 2010;35(19):10127e37.

[8] F. M. Ibanez, J. M. Echeverria, J. Vadillo, and L. Fontan, "A Step-Up Bidirectional Series Resonant DC/DC Converter Using a Continuous Current Mode," IEEE Transactions on Power Electronics, vol. 30, no. 3. pp. 1393–1402, 2015.

[9] E. Oyarbide, I. Elizondo, A. Martinez-Iturbe, C. Bernal, and J. Irisarri, "Ultracapacitor-based plug & play energy-recovery system for elevator retrofit," in 2011 IEEE International Symposium on Industrial Electronics, 2011, pp. 462–467.

[10] A. Kadavelugu, V. Baliga, S. Bhattacharya, M. Das, and A. Agarwal, "Zero Voltage Switching Performance of 1200V SiC MOSFET, 1200V Silicon IGBT and 900V CoolMOS MOSFET," 2011 IEEE Energy Conversion Congress and Exposition (Ecce), pp. 1819-1826, 2011.

[11] F. M. Ibanez, J. M. Echeverria, D. Astigarraga, and L. Fontan, "Multimode step-up bidirectional series resonant DC/DC converter using continuous current mode," IET Power Electronics, vol. 9, no. 4. pp. 710–718, 2016.

[12] D. Costinett, D. Maksimovic, and R. Zane, "Design and Control for High Efficiency in High Step-Down Dual Active Bridge Converters Operating at High Switching Frequency" IEEE Transactions on Power Electronics, vol. 28, pp. 3931-3940, Aug 2013.

[13] A. Kadavelugu, S. Baek, S. Dutta, S. Bhattacharya, M. Das, A. Agarwal, and J. Scofield, "High-frequency design considerations of dual active bridge 1200 V SiC MOSFET DC-DC converter," in 2011 Twenty-Sixth Annual IEEE Applied Power Electronics Conference and Exposition (APEC), 2011, pp. 314–320.

[14] B. Zhao, Q. Song, and W. Liu, "Experimental Comparison of Isolated Bidirectional DC–DC Converters Based on All-Si and All-SiC Power Devices for Next-Generation Power Conversion Application," IEEE Trans. Ind. Electron., vol. 61, no. 3, pp. 1389–1393, Mar. 2014.

[15] G. Y. Wang, A. Huang, and C. S. Li, "ZVS Range Extension of 10A 15kV SiC MOSFET Based 20kW Dual Active Half Bridge (DHB) DC-DC Converter," 2012 IEEE Energy Conversion Congress and Exposition (Ecce), pp. 1533-1539, 2012.

[16] J. Everts, F. Krismer, J. Van den Keybus, J. Driesen, and J. W. Kolar, "Comparative Evaluation of Soft-Switching, Bidirectional, Isolated AC/DC Converter Topologies," 2012 Twenty-Seventh Annual Ieee Applied Power Electronics Conference and Exposition (Apec), pp. 1067-1074, 2012.

[17] A. Agarwal, M. Das, B. Hull, S. Krishnaswami, J. Palmour, J. Richmond, S. Ryu, and J. Zhang, "Progress in Silicon Carbide Power Devices," in 2006 64th Device Research Conference, 2006, pp. 155–158.

[18] F. Krismer and J. W. Kolar, "Closed Form Solution for Minimum Conduction Loss Modulation of DAB Converters," IEEE Transactions on Power Electronics, vol. 27, pp. 174-188, Jan 2012.